Available online at www.sciencedirect.com
ScienceDirect
Journal of Sound and Vibration 323 (2009) 366–384
JOURNAL OF SOUND AND VIBRATION
www.elsevier.com/locate/jsvi

Free vibration analysis of rotating thick plates

S.H. Hashemi[a], S. Farhadi[a,*], S. Carra[b]

[a]*Impact Laboratory, School of Mechanical Engineering, Iran University of Science and Technology, 16846-13114 Narmak, Tehran, Iran*
[b]*Industrial Engineering Department, University of Parma, Via G.P. Usberti 181/A, 43100 Parma, Italy*

Received 12 March 2007; received in revised form 3 December 2008; accepted 4 December 2008
Handling Editor: C.L. Morfey
Available online 23 January 2009

Abstract

A finite element formulation for vibration analysis of rotating thick plates is developed. Mindlin plate theory combined with second order strain–displacement assumptions are applied for plate modeling. Kane dynamic method is employed for the derivation of nonlinear governing equations of motion, which include Coriolis effects and the couplings between in-plane and out of plane deformations. The nonlinear equations of motion are linearized using the conventional quasi static method and frequency results are obtained. The effects of different parameters including aspect ratio, thickness ratio, hub radius ratio and rotation speed on dimensionless natural frequencies are investigated and discussed. In addition, the differences between linear and nonlinear approaches toward in-plane vibration analysis of rotating plates are studied. Tune speeds are observed for the in-plane vibration frequencies. The results are in good agreement with those of other theories and experiments.

1. Introduction

Rotating structures, like blades, are common elements that are of considerable technical significance in industrial applications like rotor craft and turbomachinery. The knowledge of natural frequencies and mode shapes of these structures is essential in the design stages for studying their dynamical behavior on resonance and for flutter analysis.

The modal characteristics of elastic structures change significantly when the structures undergo overall motions. For example, centrifugal inertia forces considerably increase transverse bending frequencies of rotating beams and blades, while Coriolis effects produce vibration couplings between different vibration modes and generate complex vibration mode shapes.

Rotating blades are commonly modeled as rotating beams. This modeling enables researchers to obtain accurate modal characteristics for the structure. In early 1920, Southwell and Gough [1] investigated the vibrations of a rotating beam. Starting from the Rayleigh energy theorem, they suggested a simple algebraic equation to obtain bending natural frequencies of a rotating beam. This equation, which is often known as Southwell's equation, is still being used by many engineers due to its simplicity and accuracy. Southwell's

*Corresponding author.
E-mail address: sirwan@iust.ac.ir (S. Farhadi).

0022-460X/$ - see front matter © 2008 Elsevier Ltd. All rights reserved.
doi:10.1016/j.jsv.2008.12.007

method was later improved by Schilhansl [2]. He derived a partial differential equation of a rotating beam and applied to it the Ritz method in order to obtain more accurate coefficients for the Southwell equation. In the recent years, powerful computational methods available by modern computers make possible for researchers to employ more accurate hence complicated methods for vibration analysis of rotating beams and blades, in order to obtain more precise values of natural frequencies and mode shapes (as reported in Refs. [3–11]).

Although beam type structures can be used as a good model for lots of rotating structures like turbine blades, these models are inaccurate for investigating higher frequencies and for modeling short blades. Rotating plates are considered as better models for this type of structures [12,13]. In spite of the need, only a few research papers on the vibration analysis of rotating plates can be found in literature. Dokainish and Rawtani [14] used a finite element technique to determine the natural frequencies and the mode shapes of a cantilever plate mounted on a rotating disc and studied the effect of aspect ratio, speed of rotation, disc radius and setting angle on the natural frequencies. Coriolis and gyroscopic effects were not considered in their formulation. Karmakar and Sinha [15] introduced a finite element method for vibration analysis of rotating laminated composite pretwisted cantilever plates and developed a composite shell element for their modeling. They investigated the effects of pretwist angle, thickness ratio, fiber orientation, aspect ratio, skew angle and precone angle on the natural frequencies of graphite/epoxy plates. Ramamurti and Kielb [16] used a similar approach in order to determine the modal characteristics of twisted rotating plates. Using the stretch deformation terms instead of the conventional axial deformation terms, Yoo and Kim [13,17] and Yoo and Pierre [18], derived linearized equations of motion for the free vibration analysis of rotating cantilever plates in a direct way and investigated the effects of the dimensionless parameters on the modal characteristics of rotating cantilever plates. They showed that the results obtained by using this modeling method are in reasonable agreement with those obtained by the Southwell method.

Most of the studies introduced in literature are anyway based on the classical thin plate theory, which limits the application to thin plate structures. This paper is instead aimed to present an accurate model for rotating moderately thick blades with low aspect ratio. For this purpose, the blade is modeled as a rotating cantilever thick plate and a finite element formulation method for vibration analysis of this type of structures is presented. Mindlin [19] assumptions are considered for the thick plate modeling. Mindlin plate theory, or so-called first order shear deformation plate theory, incorporates the effects of rotary inertia and transverse shear deformations; thus, it yields more accurate results for vibration analysis of moderately thick plates in comparison with classical plate theory. According to the knowledge of the authors, Karmakar and Sinha [15] employed first order shear deformation plate theory, but they studied only the fundamental frequency (i.e. the first bending mode) of laminated composite plates and they mainly focused on the effect of laminate setting angels on the plate vibrations. In our work, different kinds of natural frequencies, associated to bending, torsional and in-plane modes, are investigated. In order to include the coupling effects between stretching and bending deformations in the governing equations, second order strain–displacement terms are applied. Since the structure is in a overall motion resulted from rotation around a fixed axis with a hub, which can be considered a special case of rigid body motion, the nonlinear equations of motion are derived using Kane [20] method, which is in fact known as particularly suitable for multi-body dynamics involving rigid body motion with elastic mode of distortion. In this way, inertial accelerations resulted from overall motions of the structure can be taken into account very easily. Coriolis and gyroscopic effects are included in these nonlinear equations. Then, the equations of motion are linearized around the system's stationary state. For this purpose, firstly, the displacement field components are separated into static and dynamic components and then static displacement components are calculated through equations of motion. Finally, a dynamic stiffness matrix is introduced using these static displacement components. Linear equations introduced by means of this quasi-static method do not contain the coupling effects between in-plane and out of plane deformations any more whereas the coupling effects between in-plane modes are preserved.

After verifying the model by comparison with results (for some special cases) available in the international literature, the effects of different parameters, as plate aspect ratio, thickness ratio, hub radius ratio and dimensionless rotation speed, on modal characteristics of the plate are discussed.

The Kane method was also used by Yoo et al. [13,17,18], but in that study they used a curvilinear coordinates system that simplifies the computational procedure. This method, however, seems not to be easy to be applied on structures with complex geometries. Therefore, we have preferred to use the classical coordinate systems, which could be simply applied to more complicated structures in future studies. For this

reason, in the present work, Cartesian coordinate components are employed in derivation of equations of motions. Since lots of external system excitations are introduced in the Cartesian coordinates (e.g. aerodynamic surface pressure introduced by aerodynamic piston theory), the equations of motion presented in this paper (in both linear and nonlinear form) can be employed in other applications very easily, e.g. for analysis of linear flutter or aerodynamic limit cycle oscillations of turbine blades.

In addition, these equations of motion can be applied for studying large-amplitude nonlinear vibrations of rotating plate structures, where the introduction of transverse shear deformations and rotary inertia in the mathematical modeling is of high importance but they are neglected in the classical plate theory.

It is known from other research works (see Refs. [21,22]) that in-plane vibration nonlinearities which result in an in-plane dynamic stiffness, have a considerable roll in vibration behavior of rotating structures. Effect of in-plane vibration nonlinearities is neglected in the other research papers addressed in the previous paragraphs. In this paper, linear and nonlinear approaches toward in-plane vibration analysis of rotating plates are employed and compared to each other and some useful and new results are presented.

By applying proper changes, the finite element formulation presented in this paper can be also easily used for vibration analysis of other rotating structural elements.

According to our survey in the published papers in the subject, this is the first time that a detailed discussion on in-plane vibration and buckling behavior of rotating plates is presented. It is worth mentioning that in-plane frequencies can be of great importance for thick and imperfect rotating plates, where in-plane and out-of-plane vibration couplings can produce more complicated phenomena. Moreover, these kinds of couplings can be even more important where an imperfect plate structure is rotating in a fluid medium and aeroelastic couplings, along with couplings between in-plane and out-of-plane vibration modes, affect the plate stability radically and particular attention should be paid.

2. Governing equations

Fig. 1 shows a rotating cantilever thick plate with length a, width b, thickness h, density ρ and hub radius R. The plate is rotating around an axis perpendicular to its surface with constant rotation speed Ω. A local Cartesian coordinate system xyz is fixed to the mid plane of the plate where x and y axes are, respectively, along the plate length and width and z axis is perpendicular to the plate and parallel to the rotation axis.

The angular speed $\mathbf{\Omega}$ of the plate is expressed in vector form as reported below:

$$\mathbf{\Omega} = \Omega \mathbf{e_3}, \tag{1}$$

where $\mathbf{e_3}$ is the unit vector along z axis.

The displacement vector of a generic point P of the plate in the local coordinates system is denoted by $\mathbf{u}$:

$$\mathbf{u} = ue_1 + ve_2 + we_3, \tag{2}$$

where $\mathbf{e_1}$ and $\mathbf{e_2}$ are the unit vectors along x and y axis and fixed to the plate and u, v and w are the displacement field components along the x, y and z axis, respectively.

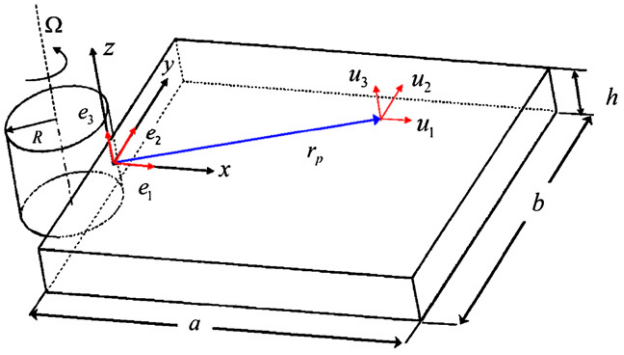

Fig. 1. Configuration of a rotating thick rectangular plate.

The velocity and acceleration vectors of the point respect to the global coordinates can be obtained as

$$\mathbf{v_P} = [\dot{u} - (y+v)\Omega]e_1 + [\dot{v} + (R+x+u)\Omega]e_2 + we_3, \tag{3}$$

$$\mathbf{a_P} = [\ddot{u} - (R+x+u)\Omega^2 - 2\Omega\dot{v}]e_1 + [\ddot{v} - (y+v)\Omega^2 + 2\Omega\dot{u}]e_2 + \ddot{w}e_3. \tag{4}$$

According to the Kane dynamic method [20], the equations of motion for vibration analysis of an elastic structure are as follows:

$$\mathbf{F}^* + \mathbf{F} = \mathbf{0}, \tag{5}$$

where **F*** and **F** are vectors of the generalized inertia forces and the generalized active forces, respectively, and are defined as

$$\mathbf{F}^* = \int_V \rho \frac{\partial v_P}{\partial \dot{q}} \cdot \mathbf{a}_P \, \mathrm{d}V, \quad \mathbf{F} = \frac{\partial U}{\partial q}. \tag{6a,b}$$

In the above equation, $\dot{\mathbf{q}}$ stands for time derivative of the generalized coordinates vector **q** and U is the strain energy of the structure and is obtained as follows:

$$U = \frac{1}{2}\int_V \varepsilon^{\mathrm{T}} \mathbf{C}\boldsymbol{\varepsilon} \, \mathrm{d}V, \tag{7}$$

where **C** is the material stiffness matrix, as introduced in Appendix A, for an isotropic Mindlin plate and **ε** and V are vector of strain components and volume of the structure, respectively.

In order to obtain the generalized inertia forces reported in Eq. (6a), the velocity and acceleration vectors (i.e. $\mathbf{v_p}$ and $\mathbf{a_p}$) must be expressed in terms of the generalized coordinates vector **q**. According to the first order shear deformation plate theory, displacement components of any generic point is obtained as shown below:

$$u = u_0 + z\theta_x = \mathbf{H_1 d}, \quad v = v_0 + z\theta_y = \mathbf{H_2 d}, \quad w = w_0 = \mathbf{H_3 d}, \tag{8}$$

where

$$\mathbf{H_1} = [1 \;\; 0 \;\; 0 \;\; z \;\; 0], \quad \mathbf{H_2} = [0 \;\; 1 \;\; 0 \;\; z \;\; 0], \quad \mathbf{H_3} = [0 \;\; 0 \;\; 1 \;\; 0 \;\; 0] \tag{9}$$

and

$$\mathbf{d} = [u_0 \;\; v_0 \;\; w_0 \;\; \theta_x \;\; \theta_y]^{\mathrm{T}}. \tag{10}$$

In the above equation, u_0, v_0 and w_0 are the displacement field components of the mid-surface of the plate and θ_x and θ_y are the rotations of the plate cross-sections normal to the mid-surface around y and x axes, respectively. Using Ritz method, the displacement and rotation components of the plate can be approximated as

$$u_0 = \sum_{j=1}^{N_1}\sum_{i=1}^{M_1} a_{i+(j-1)M_1} G_1(x,y)\Phi_i(x)\Psi_j(y),$$

$$v_0 = \sum_{j=1}^{N_2}\sum_{i=1}^{M_2} b_{i+(j-1)M_2} G_2(x,y)\Phi_i(x)\Psi_j(y),$$

$$w_0 = \sum_{j=1}^{N_3}\sum_{i=1}^{M_3} c_{i+(j-1)M_3} G_3(x,y)\Phi_i(x)\Psi_j(y),$$

$$\theta_x = \sum_{j=1}^{N_4}\sum_{i=1}^{M_4} f_{i+(j-1)M_4} G_4(x,y)\Phi_i(x)\Psi_j(y),$$

$$\theta_y = \sum_{j=1}^{N_5}\sum_{i=1}^{M_5} g_{i+(j-1)M_5} G_5(x,y)\Phi_i(x)\Psi_j(y), \tag{11}$$

where coefficients $a_{i+(j-1)\mathbf{M_1}}, \ldots$ and $g_{i+(j-1)\mathbf{M_5}}$, and are time dependent coefficients, functions $\Phi_i(x)$ and $\Psi_j(y)$ are arbitrary functions, functions $G_i(x,y)$ are manipulator functions satisfying geometrical boundary conditions and $N_1,N_2,\ldots,N_5$ and $M_1,M_2,\ldots,M_5$ are the number of terms used in the approximations functions in x and y directions, respectively. For a plate cantilevered in $x=0$, the manipulator functions are obtained as $G_i(x,y)=x$, $i=1,2,\ldots,5$. For convenience, the above assumed displacement functions are expressed in matrix form as

$$\mathbf{d}=\begin{Bmatrix} u_0 \\ v_0 \\ w_0 \\ \theta_x \\ \theta_y \end{Bmatrix}=\mathbf{Nq}, \quad \theta=\begin{Bmatrix} \mathbf{a} \\ \mathbf{b} \\ \mathbf{c} \\ \mathbf{f} \\ \mathbf{g} \end{Bmatrix}, \tag{12}$$

where $\mathbf{N}$ is the matrix of shape functions, $\mathbf{q}$ is the generalized coordinates vector and $\mathbf{a}$, $\mathbf{b}$, $\mathbf{c}$, $\mathbf{g}$ and $\mathbf{h}$ are vectors which are made of the corresponding time dependent coefficients reported in Eq. (11). Substituting Eq. (12) into Eq. (10) and differentiating with respect to time, the following equations are obtained:

$$\dot{u}=\mathbf{H_1N}\dot{\mathbf{q}}=\mathbf{L_1}\dot{\mathbf{q}},$$

$$\dot{v}=\mathbf{H_2N}\dot{\mathbf{q}}=\mathbf{L_2}\dot{\mathbf{q}},$$

$$\dot{w}=\mathbf{H_3N}\dot{\mathbf{q}}=\mathbf{L_3}\dot{\mathbf{q}}. \tag{13}$$

Differentiating the above equations with respect to $\dot{\mathbf{q}}$ gives

$$\frac{\partial \dot{u}}{\partial \dot{\mathbf{q}}}=\mathbf{L}_1^{\mathrm{T}}, \quad \frac{\partial \dot{v}}{\partial \dot{\mathbf{q}}}=\mathbf{L}_2^{\mathrm{T}}, \quad \frac{\partial \dot{w}}{\partial \dot{\mathbf{q}}}=\mathbf{L}_3^{\mathrm{T}}. \tag{14}$$

Thus, by substituting the above equations in Eq. (6a), the generalized inertia forces are obtained as shown below:

$$\mathbf{F}^*=\mathbf{Fs_1}\ddot{\mathbf{q}}+\mathbf{Fs_2}\dot{\mathbf{q}}+\mathbf{Fs_3q}+\mathbf{Fs_4}, \tag{15}$$

where

$$\mathbf{Fs_1}=\rho\int_V(\mathbf{L_1^TL_1}+\mathbf{L_2^TL_2}+\mathbf{L_3^TL_3})\,\mathrm{d}V, \tag{16}$$

$$\mathbf{Fs_2}=2\rho\Omega\int_V(-\mathbf{L_1^TL_2}+\mathbf{L_2^TL_2})\,\mathrm{d}V, \tag{17}$$

$$\mathbf{Fs_3}=\rho\Omega^2\int_V(-\mathbf{L_1^TL_1}-\mathbf{L_2^TL_2})\,\mathrm{d}V, \tag{18}$$

$$\mathbf{Fs_4}=\rho\Omega^2\int_V(-(R+x)\mathbf{L_1^T}-y\mathbf{L_2^T})\,\mathrm{d}V. \tag{19}$$

In order to obtain the generalized active forces, the components of strain tensor should be obtained in terms of generalized coordinates vector. According to the first order shear deformation plate theory, the plate normal strain in direction normal to the plate (i.e. ε_{zz}) is negligible and thus the vector of the strain tensor components, i.e. ε, is obtained as follows:

$$\boldsymbol{\varepsilon}=[\varepsilon_{xx}\ \ \varepsilon_{yy}\ \ \varepsilon_{yz}\ \ \varepsilon_{xz}\ \ \varepsilon_{zy}]^{\mathrm{T}}. \tag{20}$$

According to Mindlin plate theory and by adding Von Karman second order strain–displacement terms, the components of the strain tensor are defined as:

$$\varepsilon_{xx}=\frac{\partial u_0}{\partial x}+\frac{1}{2}\left(\frac{\partial w_0}{\partial x}\right)^2+z\frac{\partial \theta_x}{\partial x},$$

$$\varepsilon_{yy} = \frac{\partial v_0}{\partial y} + \frac{1}{2}\left(\frac{\partial w_0}{\partial y}\right)^2 + z\frac{\partial \theta_y}{\partial y},$$

$$\varepsilon_{yz} = \frac{\partial w_0}{\partial y} + \theta_y,$$

$$\varepsilon_{xz} = \frac{\partial w_0}{\partial x} + \theta_x,$$

$$\varepsilon_{xy} = \frac{\partial u_0}{\partial y} + \frac{\partial v_0}{\partial x} + \left(\frac{\partial w_0}{\partial x}\frac{\partial w_0}{\partial y}\right) + z\left(\frac{\partial \theta_x}{\partial y} + \frac{\partial \theta_y}{\partial x}\right). \tag{21a}$$

The full nonlinear version of strain components can be presented as follows:

$$\varepsilon_{xx} = \frac{\partial u}{\partial x} + \frac{1}{2}\left(\frac{\partial u}{\partial x}\right)^2 + \frac{1}{2}\left(\frac{\partial v}{\partial x}\right)^2 + \frac{1}{2}\left(\frac{\partial w}{\partial x}\right)^2,$$

$$\varepsilon_{yy} = \frac{\partial v}{\partial y} + \frac{1}{2}\left(\frac{\partial u}{\partial y}\right)^2 + \frac{1}{2}\left(\frac{\partial v}{\partial y}\right)^2 + \frac{1}{2}\left(\frac{\partial w}{\partial y}\right)^2,$$

$$\varepsilon_{yz} = \frac{\partial v}{\partial z} + \frac{\partial w}{\partial y} + \frac{\partial u}{\partial z}\frac{\partial u}{\partial y} + \frac{\partial v}{\partial z}\frac{\partial v}{\partial y} + \frac{\partial w}{\partial z}\frac{\partial w}{\partial y},$$

$$\varepsilon_{xz} = \frac{\partial u}{\partial z} + \frac{\partial w}{\partial x} + \frac{\partial u}{\partial z}\frac{\partial u}{\partial x} + \frac{\partial v}{\partial z}\frac{\partial v}{\partial x} + \frac{\partial w}{\partial z}\frac{\partial w}{\partial x},$$

$$\varepsilon_{xy} = \frac{\partial u}{\partial y} + \frac{\partial v}{\partial x} + \frac{\partial u}{\partial x}\frac{\partial u}{\partial y} + \frac{\partial v}{\partial x}\frac{\partial v}{\partial y} + \frac{\partial w}{\partial x}\frac{\partial w}{\partial y}, \tag{21b}$$

where u, v and w are defined by Eq. (8).

By separating the strain components in Eq. (21a) into linear and nonlinear parts, linear and nonlinear strain vectors can be defined:

$$\boldsymbol{\varepsilon} = \boldsymbol{\varepsilon}_{\mathbf{l}} + \boldsymbol{\varepsilon}_{\mathbf{nl}}, \tag{22}$$

where

$$\boldsymbol{\varepsilon}_{\mathbf{l}} = \begin{Bmatrix} \dfrac{\partial u_0}{\partial x} + z\dfrac{\partial \theta_x}{\partial x} \\ \dfrac{\partial v_0}{\partial y} + z\dfrac{\partial \theta_y}{\partial y} \\ \dfrac{\partial w_0}{\partial y} + \theta_y \\ \dfrac{\partial w_0}{\partial x} + \theta_x \\ \dfrac{\partial u_0}{\partial y} + \dfrac{\partial v_0}{\partial x} + z\left(\dfrac{\partial \theta_x}{\partial y} + \dfrac{\partial \theta_y}{\partial x}\right) \end{Bmatrix}, \quad \boldsymbol{\varepsilon}_{\mathbf{nl}} = \begin{Bmatrix} \dfrac{1}{2}\left(\dfrac{\partial w_0}{\partial x}\right)^2 \\ \dfrac{1}{2}\left(\dfrac{\partial w_0}{\partial y}\right)^2 \\ 0 \\ 0 \\ \dfrac{\partial w_0}{\partial x}\dfrac{\partial w_0}{\partial y} \end{Bmatrix}. \tag{23}$$

For the case of fully nonlinear strain components (Eq. (21b)), linear strain vector is the same as introduced in Eq. (23). But the nonlinear part must be modified by including extra terms.

The linear and nonlinear strain vectors can be rewritten as

$$\boldsymbol{\varepsilon}_{\mathbf{l}} = \mathbf{S}_1\mathbf{q}, \tag{24}$$

$$\boldsymbol{\varepsilon}_{\mathbf{nl}} = [\mathbf{Q}_1\mathbf{q}\ \ \mathbf{Q}_2\mathbf{q}\ \ \cdots\ \ \mathbf{Q}_5\mathbf{q}]\mathbf{S}_2\mathbf{q}, \tag{25}$$

where

$$\mathbf{Q_i} = \mathbf{A_i N}, \quad i = 1, 2, \ldots, 5,$$

$$\mathbf{S_j} = \mathbf{B_j N}, \quad j = 1, 2. \tag{26}$$

In the above equations, $\mathbf{A_i}$ and $\mathbf{B_j}$ are operator matrices as defined in Appendix B. Eq. (25) can be rewritten as follows:

$$\boldsymbol{\varepsilon}_{\mathbf{nl}} = \mathbf{D_1^T q}, \tag{27}$$

where

$$\mathbf{D_1} = [\mathbf{S_2^T Q_1 q} \;\; \mathbf{S_2^T Q_2 q} \;\; \cdots \;\; \mathbf{S_2^T Q_5 q}]. \tag{28}$$

Substituting Eqs. (24) and (27) in Eq. (22) and, then, the obtained result in Eq. (7) and differentiating with respect to the generalized coordinates vector $\mathbf{q}$, the following expression is obtained:

$$\frac{\partial U}{\partial \mathbf{q}} = \int_V \frac{\partial \boldsymbol{\varepsilon}_\mathbf{l}^\mathrm{T}}{\partial \mathbf{q}} \mathbf{C}\boldsymbol{\varepsilon}_\mathbf{l} \, \mathrm{d}V + \int_V \left(\frac{\partial \boldsymbol{\varepsilon}_\mathbf{l}^\mathrm{T}}{\partial \mathbf{q}} \mathbf{C}\boldsymbol{\varepsilon}_\mathbf{n} + \frac{\partial \boldsymbol{\varepsilon}_\mathbf{n}^\mathrm{T}}{\partial \mathbf{q}} \mathbf{C}\boldsymbol{\varepsilon}_\mathbf{l} \right) \mathrm{d}V + \int_V \frac{\partial \boldsymbol{\varepsilon}_\mathbf{n}^\mathrm{T}}{\partial \mathbf{q}} \mathbf{C}\boldsymbol{\varepsilon}_\mathbf{n} \, \mathrm{d}V. \tag{29}$$

Differentiating Eqs. (24) and (27) with respect to the generalized coordinates vector $\mathbf{q}$, the following equations are obtained:

$$\frac{\partial \boldsymbol{\varepsilon}_\mathbf{1}^\mathrm{T}}{\partial \mathbf{q}} = \mathbf{S_1^T}, \quad \frac{\partial \boldsymbol{\varepsilon}_\mathbf{nl}^\mathrm{T}}{\partial \mathbf{q}} = \mathbf{D_1} + \mathbf{D_2}, \tag{30a,b}$$

where $\mathbf{D_1}$ is defined as in Eq. (28) and $\mathbf{D}_2$ is defined as follows:

$$\mathbf{D_2} = [\mathbf{Q_1^T S_2 q} \;\; \mathbf{Q_2^T S_2 q} \;\; \cdots \;\; \mathbf{Q_5^T S_2 q}]. \tag{31}$$

Thus, by substituting Eq. (29) in Eq. (6b) and using Eqs. (30a,b), the generalized active forces are defined:

$$\mathbf{F} = \frac{\partial U}{\partial \mathbf{q}} = (\mathbf{F_1} + \mathbf{F_2} + \mathbf{F_3})\mathbf{q}, \tag{32}$$

where

$$\mathbf{F_1} = \int_V \mathbf{S_1^T C S_1} \, \mathrm{d}V,$$

$$\mathbf{F_2} = \int_V (\mathbf{S_1^T C D_1^T} + (\mathbf{D_1} + \mathbf{D_2})\mathbf{C S_1}) \, \mathrm{d}V,$$

$$\mathbf{F_3} = \int_V (\mathbf{D_1} + \mathbf{D_2})\mathbf{C D_1^T} \, \mathrm{d}V. \tag{33}$$

It should be noticed that in the above equations $\mathbf{F_2}$ and $\mathbf{F_3}$ are nonlinear stiffness matrices which are dependent on the generalized coordinates vector $\mathbf{q}$.

By using the components of Eq. (5) reported in Eqs. (15) and (32), the nonlinear equations of motion for free vibration of the rotating plate can be written as shown below:

$$\mathbf{M\ddot{q}} + \mathbf{CD\dot{q}} + (\mathbf{K} + \mathbf{K_q} + \mathbf{K_{qq}})\mathbf{q} + \mathbf{Fs_4} = \mathbf{0}, \tag{34}$$

where

$$\mathbf{M} = \mathbf{Fs_1}, \quad \mathbf{CD} = \mathbf{Fs_2}, \quad \mathbf{K} = \mathbf{Fs_3} + \mathbf{F_1}, \quad \mathbf{K_q} = \mathbf{F_2}, \quad \mathbf{K_{qq}} = \mathbf{F_3}. \tag{35}$$

In the above equation, $\mathbf{K_q}$ and $\mathbf{K_{qq}}$ are nonlinear stiffness matrices which are dependent on the generalized coordinates vector $\mathbf{q}$.

For free vibration analysis of non-rotating thick plates, one can simply substitute $\Omega = 0$ in Eqs. (17)–(19) and omit the nonlinear stiffness matrices. Thus, the equations of motion for this case are obtained as

$$\mathbf{M\ddot{q}} + \mathbf{Kq} = \mathbf{0}, \tag{36}$$

where

$$\mathbf{M} = \mathbf{Fs_1}, \quad \mathbf{K} = \mathbf{F_1}. \tag{37}$$

Assuming the generalized coordinates vector to be harmonic ($\mathbf{q} = \overline{\mathbf{q}}e^{i\omega t}$), Eq. (36) reduces to a conventional eigenvalue problem which will yields natural frequencies and mode shapes of a non-rotating thick plate.

3. Linearization of the governing equation

At this stage, in order to linearize Eq. (34), the generalized coordinates vector is separated into static and dynamic components as shown below:

$$\mathbf{q} = \mathbf{q_s} + \mathbf{q_d}, \tag{38}$$

where $\mathbf{q_s}$ and $\mathbf{q_d}$ represent static and dynamic parts of the generalized coordinates vector, respectively. Since Eq. (34) is a general equation of motion, it should be satisfied by substituting $\mathbf{q} = \mathbf{q_s}$ for static analysis, obtaining:

$$(\mathbf{K} + \mathbf{K}_{\mathbf{q_s}} + \mathbf{K}_{\mathbf{q_s q_s}})\mathbf{q_s} + \mathbf{Fs_4} = \mathbf{0}. \tag{39}$$

It should be mentioned that for the case of linear in-plane vibrations, $\mathbf{q_s}$ only includes in-plane non-zero terms, since the plate just undergoes in-plane static deflections resulted from centrifugal inertia forces ($\mathbf{d_s} = \mathbf{Nq_s} = [u_{0s}\ \ v_{0s}\ \ 0\ \ 0\ \ 0]^T$). Using Eqs. (28), (31), (33) and (35) and by means of the operator matrices $\mathbf{A_i}$ and $\mathbf{B_j}$ introduced in Appendix B, one can simply show that for the case of linear in-plane vibrations (Eq. (21a)):

$$\mathbf{K}_{\mathbf{q_s}}\mathbf{q_s} = \mathbf{0}, \quad \mathbf{K}_{\mathbf{q_s q_s}}\mathbf{q_s} = \mathbf{0}. \tag{40}$$

Thus, Eq. (39) reduces to a set of linear algebraic equations and $\mathbf{q_s}$ can be defined as follows:

$$\mathbf{q_s} = -\mathbf{K}^{-1}\mathbf{Fs_4}. \tag{41a}$$

For the case of full nonlinear strain components (Eq. (21b)):

$$\mathbf{q_s} = -(\mathbf{K} + \mathbf{K}_{\mathbf{q_s}} + \mathbf{K}_{\mathbf{q_s q_s}})^{-1}\mathbf{Fs_4}. \tag{41b}$$

Substituting Eq. (41) into Eq. (38) and the obtained result into Eq. (34), the following governing equation is defined:

$$\mathbf{M}\ddot{\mathbf{q}}_\mathbf{d} + \mathbf{CD}\dot{\mathbf{q}}_\mathbf{d} + \mathbf{K}\mathbf{q}_\mathbf{d} + \mathbf{K}_{\mathbf{q_d}}\mathbf{q_s} + \mathbf{K}_{\mathbf{q_S}}\mathbf{q_d} + \mathbf{K}_{\mathbf{q_d q_S}}\mathbf{q_s} + \mathbf{K}_{\mathbf{q_S q_d}}\mathbf{q_s} + \mathbf{K}_{\mathbf{q_S q_S}}\mathbf{q_d} + \mathbf{O}(\mathbf{q_d^2}) + \mathbf{O}(\mathbf{q_d^3}) = \mathbf{0}. \tag{42}$$

Above equation can be shortened by the following definition:

$$\mathbf{K}_{\mathbf{q_d}}\mathbf{q_s} + \mathbf{K}_{\mathbf{q_S}}\mathbf{q_d} + \mathbf{K}_{\mathbf{q_d q_S}}\mathbf{q_s} + \mathbf{K}_{\mathbf{q_S q_d}}\mathbf{q_s} + \mathbf{K}_{\mathbf{q_S q_S}}\mathbf{q_d} = \mathbf{K}'\mathbf{q_d}, \tag{43}$$

where $\mathbf{K}'$ is dynamic stiffness matrix. In Eq. (43) each term is calculated by using the corresponding displacement vector. For example $\mathbf{K_{qd}}$ is defined as

$$\mathbf{K}_{\mathbf{q_d}} = \int_V (\mathbf{S_1^T}\mathbf{CD}_{\mathbf{1q_d}}^{\mathrm{T}} + (\mathbf{D}_{\mathbf{1q_d}} + \mathbf{D}_{\mathbf{2q_d}})\mathbf{CS_1})\,\mathrm{d}V, \tag{44}$$

where

$$\mathbf{D_{1q_d}} = [\mathbf{S_2^T}\mathbf{Q_1}\mathbf{q_d}\ \ \mathbf{S_2^T}\mathbf{Q_2}\mathbf{q_d}\ \ \cdots\ \ \mathbf{S_2^T}\mathbf{Q_5}\mathbf{q_d}],$$

$$\mathbf{D_{2q_d}} = [\mathbf{Q_1^T}\mathbf{S_2}\mathbf{q_d}\ \ \mathbf{Q_2^T}\mathbf{S_2}\mathbf{q_d}\ \ \cdots\ \ \mathbf{Q_5^T}\mathbf{S_2}\mathbf{q_d}]. \tag{45}$$

Finally, by substituting Eq. (43) into Eq. (42) and eliminating the nonlinear terms, the following linear governing equation is defined for rotating thick plates:

$$\mathbf{M}\ddot{\mathbf{q}}_\mathbf{d} + \mathbf{CD}\dot{\mathbf{q}}_\mathbf{d} + (\mathbf{K} + \mathbf{K}')\mathbf{q_d} = \mathbf{0}. \tag{46}$$

It is worth mentioning that in Eq. (43), for the case of linear in-plane vibrations, all terms in the left side of the equation are zero, except the first term. For the case of nonlinear in-plane vibrations, three hypotheses can be assigned for definition of static displacements, namely:

I. Small static displacements: in Eqs. (41b) and (43) nonlinear terms of $\mathbf{q_s}$ are neglected.
II. Moderate static displacements: cubic nonlinear terms of Eq. (41b) and nonlinear terms of Eq. (43) are neglected.
III. Large static displacements: Eqs. (41b) and (43) are solved nonlinearly.

4. Numerical results

In order to determine the modal characteristics of rotating and non-rotating plates, the governing equation of the system (Eq. (36)) is firstly transformed into a set of first order differential equations:

$$\boldsymbol{\alpha}\dot{\mathbf{r}} + \boldsymbol{\beta}\mathbf{r} = \mathbf{0}, \tag{47}$$

where $\mathbf{r}$ is the vector of the system states, defined as

$$\mathbf{r} = \begin{Bmatrix} \dot{\mathbf{q}}_\mathbf{d} \\ \mathbf{q}_\mathbf{d} \end{Bmatrix} \tag{48}$$

and α and β are given by

$$\boldsymbol{\alpha} = \begin{bmatrix} \mathbf{M} & \mathbf{0} \\ \mathbf{0} & \mathbf{I} \end{bmatrix}, \quad \boldsymbol{\beta} = \begin{bmatrix} \mathbf{CD} & \mathbf{K}+\mathbf{K}' \\ -\mathbf{I} & \mathbf{0} \end{bmatrix}. \tag{49}$$

Subsequently, the vector of the system states is assumed to be harmonic ($\mathbf{r} = \overline{\mathbf{r}}e^{i\omega t}$) and the governing equation (Eq. (47)) is reduced to a conventional eigenvalue problem. The characteristic matrices $\mathbf{M}$, $\mathbf{CD}$, $\mathbf{K}$ and $\mathbf{K}'$ are calculated through exact analytical integrations using Mathematica software. In Eq. (49) $\mathbf{I}$ represents the identity matrix.

In the present work, power series are used as arbitrary functions ($\Phi_i(x) = x^{i-1}$ and $\Psi_j(y) = y^{j-1}$). For convenience, the approximation series in different directions are taken of the same order ($M_1 = M_2 = \cdots = M_5 = M$ and $N_1 = N_2 = \cdots = N_5 = N$). In all presented tables and figures, δ, η, σ, $\overline{\omega}$ and γ denote aspect ratio, thickness ratio, hub radius ratio, dimensionless natural frequency and dimensionless rotation speed, respectively, and are defined as shown below:

$$\delta = a/b, \quad \eta = h/a, \quad \sigma = R/a, \quad \overline{\omega} = \omega a^2\sqrt{\rho h/D}, \quad \gamma = \Omega T, \tag{50}$$

where ω and D are, respectively, a generic natural frequency and the flexural rigidity of the plate and

$$D = Eh^3/(12(1-\nu^2)), \quad T = \sqrt{\rho h a^4/D}, \tag{51}$$

where E and ν are Young's modulus of elasticity and Poisson's ratio, respectively.

For validating the governing equation obtained for non-rotating plates (i.e. Eq. (36)), a convergence study has been performed.

Table 1 presents the case of the dimensionless natural frequencies of a thick non-rotating rectangular plate with SCSC[1] boundary conditions and dimensionless ratios $\delta = 0.5$ and $\eta = 0.15$, for different values of M and N. In addition, the results are compared with exact solutions presented by Hashemi and Arsanjani [23]. It can be observed from the table that the nine first natural frequencies of the plate converge to the exact values [23] with a great precision in the case of assumed modes number $M \times N = 9 \times 9$. As it is expected from the Rayleigh–Ritz method, the results obtained by the present method for natural frequencies converge to the exact solutions from upper frequency bound as the number of assumed modes in the displacement assumption functions (i.e. M and N) increases.

[1]Simply supported-clamped–simply supported-clamped.

Table 1
Comparison of dimensionless natural frequencies obtained by the present method (for different values of N and M) and by the exact method [21] for a non-rotating thick plate with SCSC boundary conditions and dimensionless ratios $\delta = 0.5$, $\eta = 0.15$.

	Number of modes ($M \times N$)						Exact [21]	Error percent
	4×4	5×5	6×6	7×7	8×8	9×9		
$\overline{\omega}_1$	12.8672	12.8481	12.8474	12.8456	12.8456	12.8450	12.8449	0.00
$\overline{\omega}_2$	21.2813	21.2564	21.1906	21.1893	21.1861	21.1861	21.1853	0.00
$\overline{\omega}_3$	35.2198	33.3313	33.0074	32.8609	32.8519	32.8486	32.8480	0.00
$\overline{\omega}_4$	37.0489	36.9953	36.8308	36.8269	36.8241	36.8238	36.8226	0.00
$\overline{\omega}_5$	50.1377	43.6383	43.5602	43.2461	43.2427	43.2316	43.2289	0.01
$\overline{\omega}_6$	56.5685	50.7195	48.4431	47.2623	46.9989	46.9491	46.9422	0.01
$\overline{\omega}_7$	66.1986	56.5685	53.7896	53.6240	53.0529	53.0474	53.0168	0.06
$\overline{\omega}_8$	76.1577	71.5357	69.3059	66.2273	63.4926	63.0439	62.8423	0.32
$\overline{\omega}_9$	88.8387	76.1577	71.4664	67.0258	66.3783	65.5035	65.4110	0.14

The error percent is calculated between the case of $M \times N = 9 \times 9$ and the exact method [21].

Table 2
Comparison of dimensionless natural frequencies obtained by the present method (for $M \times N = 9 \times 9$) and by the exact method [21] for a non-rotating thick plate with SSSS boundary conditions.

	$\delta = 1$, $\eta = 0.1$			$\delta = 1$, $\eta = 0.2$			$\delta = 0.5$, $\eta = 0.1$		
	Present work	Exact [21]	Error percent	Present work	Exact [21]	Error percent	Present work	Exact [21]	Error percent
$\overline{\omega}_1$	19.0840	19.0840	0.00	17.5055	17.5055	0.00	12.0752	12.0752	0.00
$\overline{\omega}_2$	45.5845	45.5845	0.00	38.3847	38.3847	0.00	19.0840	19.0840	0.00
$\overline{\omega}_3$	45.5845	45.5845	0.00	38.3847	38.3847	0.00	30.4080	30.4080	0.00
$\overline{\omega}_4$	70.0219	70.0219	0.00	55.5860	55.5860	0.00	39.1713	39.1713	0.00
$\overline{\omega}_5$	85.3655	85.3654	0.00	65.7265	65.7193	0.01	45.5846	45.5845	0.00
$\overline{\omega}_6$	85.3655	85.3654	0.00	65.7265	65.7193	0.01	45.6264	45.5845	0.09
$\overline{\omega}_7$	107.2131	107.1775	0.03	79.4805	79.4758	0.01	56.0104	55.9920	0.03
$\overline{\omega}_8$	107.2131	107.1775	0.03	79.4805	79.4758	0.01	64.2916	64.0823	0.33
$\overline{\omega}_9$	134.4826	134.3586	0.09	95.8660	95.8088	0.06	70.1041	70.0219	0.12

The dimensionless natural frequencies for different geometrical characteristics of a non-rotating thick plate with SSSS[2] boundary conditions are compared with exact values [23] in Table 2. The comparison results presented in Tables 1 and 2 attest the validity of the governing equation (Eq. (34)) for non-rotating plates.

Table 3 presents a convergence study for dimensionless natural frequencies of a thick rotating cantilever plate with thickness ratio $\eta = 0.1$, aspect ratio $\delta = 3$, hub radius ratio $\sigma = 0$ and dimensionless rotation speed $\gamma = 10$. It can be observed that, for the case of $M \times N = 9 \times 9$, a good convergence for the ten lowest frequencies of the structure is achieved.

In Tables 4 and 5, the five lowest natural frequencies obtained on the basis of the present method are compared with those obtained by Yoo and Kim [13] for a cantilever rotating plate with aspect ratio $\delta = 1$, two different hub radius ratios $\sigma = 0$ and 1 and two different rotation speeds $\gamma = 1$ and 2. For this comparison, thickness ratio $\eta = 0.01$ and the hypothesis of linear in-plane motions are used for modeling thin plates. A good agreement between the two methods can be observed in the comparison results, since the differences are less than 1% for all cases. The error percentages with minus sign in Tables 4 and 5 show that the results obtained by the present method are always lower than the results obtained by Yoo and Kim [13]. It is in fact well known from the Mindlin plate theory that considering lateral shear deformations in the plate modeling results in a more flexible structure and leads the frequency results towards slightly lower values with respect to

[2]Simply supported in all edges.

Table 3
Convergence of dimensionless natural frequencies of a thick rotating cantilever rectangular plate ($\delta = 3$, $\sigma = 0$, $\gamma = 10$, $\eta = 0.1$).

Number of modes ($M \times N$)	$\overline{\omega}_1$	$\overline{\omega}_2$	$\overline{\omega}_3$	$\overline{\omega}_4$	$\overline{\omega}_5$	$\overline{\omega}_6$	$\overline{\omega}_7$	$\overline{\omega}_8$	$\overline{\omega}_9$	$\overline{\omega}_{10}$
3×3	3.302	11.277	23.246	32.445	47.064	55.876	69.789	85.632	131.241	136.089
4×4	2.881	11.249	22.623	32.432	46.490	55.715	62.386	68.136	107.986	124.651
5×5	2.744	11.243	22.436	32.374	45.613	55.562	61.401	67.728	106.132	107.159
6×6	2.674	11.242	22.362	32.352	45.484	55.533	61.113	67.340	103.987	104.136
7×7	2.636	11.241	22.343	32.348	45.441	55.519	60.914	67.285	103.648	103.737
8×8	2.615	11.240	22.335	32.344	45.408	55.508	60.873	67.265	103.304	103.665
9×9	2.602	11.239	22.331	32.341	45.390	55.500	60.865	67.258	103.252	103.609

Table 4
Comparison of the five lowest natural frequencies obtained by the present method and by Yoo and Kim [13] ($\delta = 1$, $\sigma = 0$).

	$\gamma = 1$			$\gamma = 2$		
	Present method	Yoo and Kim [13]	Error percent	Present method	Yoo and Kim [13]	Error percent
$\overline{\omega}_1$	3.6437	3.6528	−0.2493	4.1051	4.11312	−0.1951
$\overline{\omega}_2$	8.6289	8.6459	−0.1963	8.9790	9.00317	−0.2690
$\overline{\omega}_3$	21.4378	21.53372	−0.4453	21.8630	21.96654	−0.4713
$\overline{\omega}_4$	27.2592	27.38478	−0.4587	27.4993	27.62312	−0.4483
$\overline{\omega}_5$	31.0695	31.21853	−0.4775	31.4258	31.58544	−0.5055

A thickness ratio $\eta = 0.01$ is used for modeling thin plates.

Table 5
Comparison of the five lowest natural frequencies obtained by the present method and by Yoo and Kim [13] ($\delta = 1$, $\sigma = 1$).

	$\gamma = 1$			$\gamma = 2$		
	Present method	Yoo and Kim [13]	Error percent	Present method	Yoo and Kim [13]	Error percent
$\overline{\omega}_1$	3.8532	3.86185	−0.2241	4.8069	4.81385	−0.1441
$\overline{\omega}_2$	8.7157	8.73585	−0.2302	9.3079	9.34355	−0.3814
$\overline{\omega}_3$	21.6205	21.71968	−0.4567	22.5615	22.67981	−0.5217
$\overline{\omega}_4$	27.3009	27.42572	−0.4551	27.6713	27.79012	−0.4277
$\overline{\omega}_5$	31.2101	31.3624	−0.4856	31.9771	32.14933	−0.5358

A thickness ratio $\eta = 0.01$ is used for modeling thin plates.

the ones obtained by the classical plate theory (Kirchhoff theory). In other words, the classical plate theory overestimates the structural dynamic characteristics.

Fig. 2 shows the variations of the three lowest dimensionless bending frequencies, the two lowest dimensionless torsional frequencies and the first in-plane dimensionless frequency of a non-rotating plate versus the plate aspect ratio. Results are plotted for different thickness ratios. As it can be observed in the figure, in all cases, bending frequencies remain constant, torsional frequencies increase and in-plane frequencies decrease as the aspect ratio increases. The variation of the torsional frequencies versus aspect ratio seems to be linear for thin plates ($\eta = 0.01$), whereas such a trend is not confirmed for thick plates (e.g. $\eta = 0.1$ and 0.15). In addition, it can be observed that all the frequencies decrease as the thickness ratio increases and that, for higher thickness ratios, the in-plane frequencies have a more significant shift towards lower values with respect to bending and torsional frequencies.

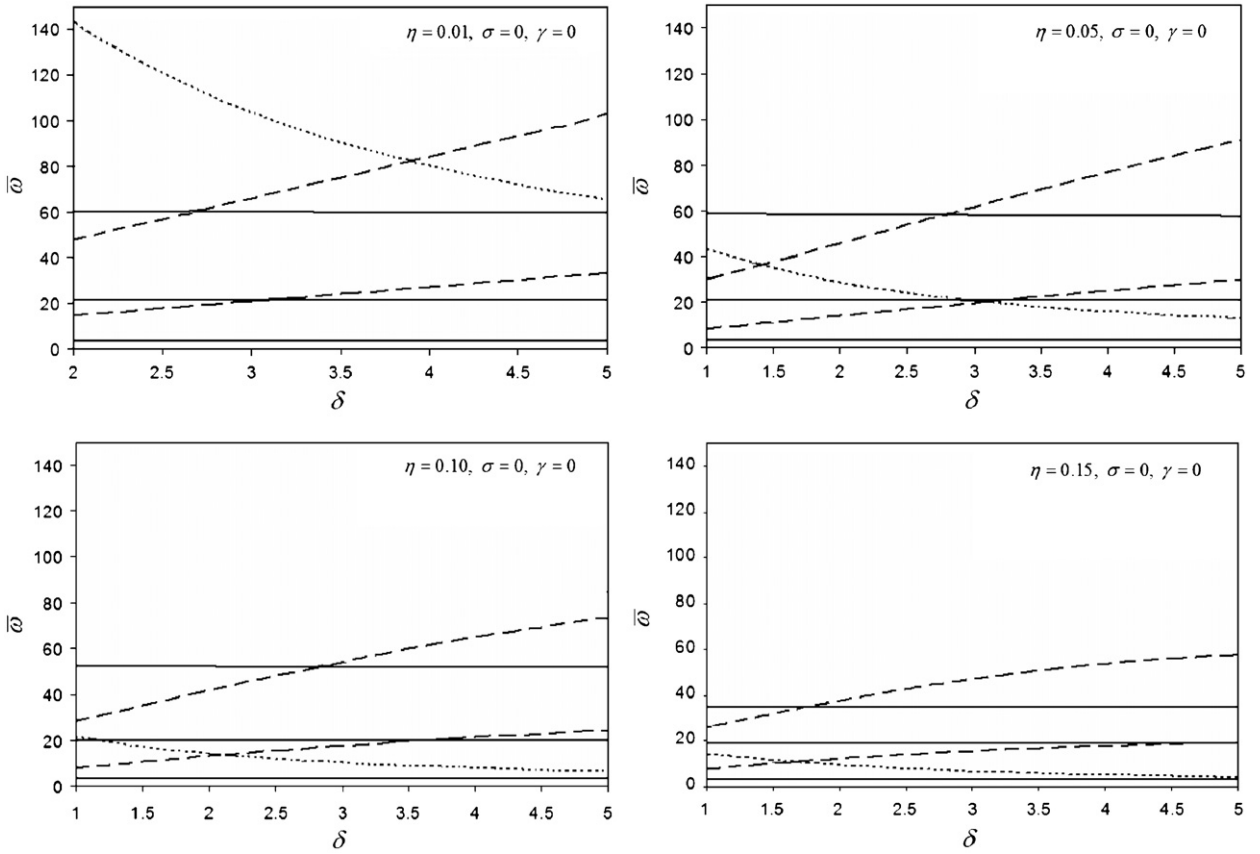

Fig. 2. Variations of the dimensionless natural frequencies of non-rotating plates versus aspect ratio (δ) for different values of the thickness ratio (η); — bending modes, - - torsional modes, and ..... in-plane modes.

Fig. 3 reports, as an example, the mode shapes corresponding to third bending mode, second torsional mode and first in-plane mode of a non-rotating plate with aspect ratios $\delta = 1.5$ and 4, respectively.

Fig. 4 shows the variations of the lowest dimensionless natural frequencies of a rotating plate ($\gamma = 1$) versus thickness ratio for different aspect ratios. It can be clearly observed from this figure (as mentioned before) that all natural frequencies decrease as thickness ratio increases, but this trend is more significant for in-plane vibration modes. This phenomenon appears for all the values of thickness ratio. It can be also observed that, for increasing values of the aspect ratio δ, the in-plane frequencies progressively move towards lower frequency bands with respect to bending and torsional ones.

The variations of the dimensionless natural frequencies versus dimensionless rotation speed for different thickness ratios are plotted in Fig. 5. It can be observed from the figure that the out-of-plane frequencies increase as the rotation speed increases, whereas in-plane frequencies decrease and plate buckles in the higher rotation speeds (γ_b). It is worth mentioning that buckling of in-plane modes is due to Coriolis effects. From the figure it can be seen that the buckling dimensionless speed γ_b depends on thickness ratio and decreases as the thickness ratio increases. It can be also realized from the figure that there are some critical speeds in which the plate rotation speed becomes equal to in-plane vibration frequency (points A and B in Fig. 5, where the in-plane frequencies loci cross line $\gamma = \overline{\omega}$). These rotations speeds, or so called tune speeds, should be avoided in design procedure, since unbalances in the rotor system can lead the structure to resonance at these speeds. According to the figure, tune speeds decrease as the plate thickness ratio increases. Fig. 5 also shows the eigenvalue loci veering for out-of-plane frequencies and the eigenvalue loci crossing between out-of-plane

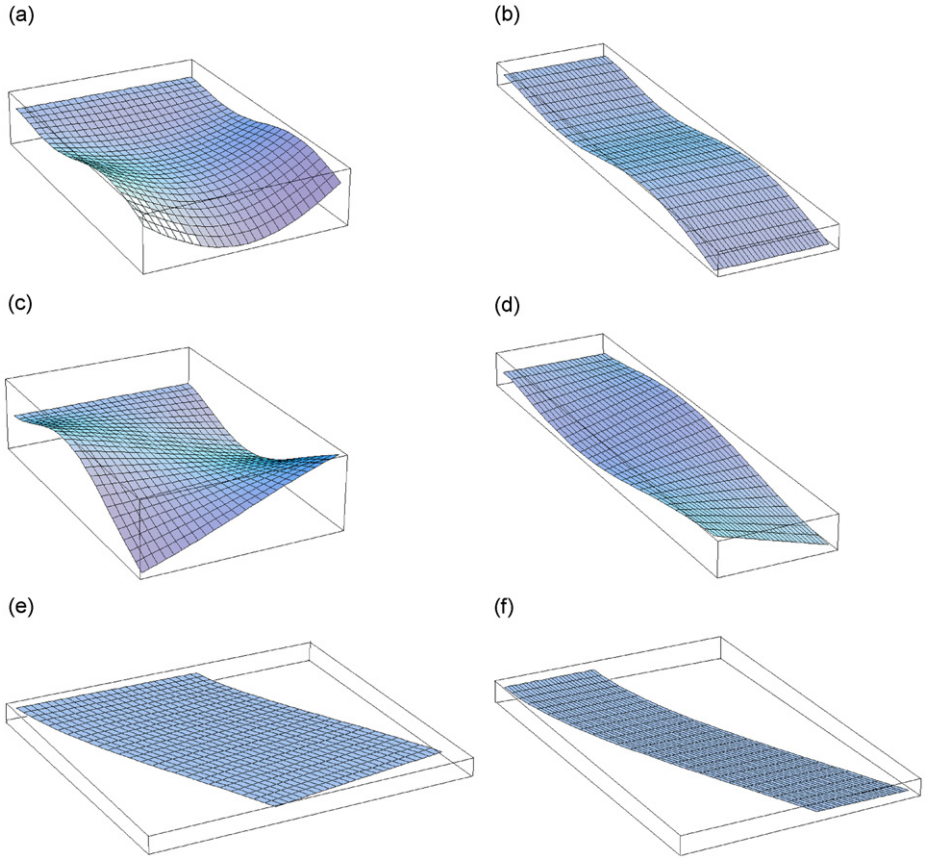

Fig. 3. Mode shapes corresponding to third bending mode (cases (a) and (b)), second tortional mode (cases (c) and (d)) and first in-plane mode (cases (e) and (f)) of a non-rotating plate with aspect ratio $\delta = 1.5$ and 4, respectively.

frequencies and also between in-plane and out-of-plane frequencies. A detailed discussion about these phenomena can be found in Ref. [13].

In a study about in-plane vibration of rotating disks, Deshpande and Mote [21] showed that in-plane buckling of rotating structures, which is reported in different previous studies, is due to linear analysis of in-plane vibrations and is not correct. In fact in order to have correct prediction of in-plane vibration frequencies of rotating structures, it is essential to introduce second order derivatives of in-plane displacement components in to the structure strain components (Eq. (21b)), which results in an in-plane dynamic stiffness for the structure.

Fig. 6 illustrates in-plane vibration frequencies of a rotating plate with dimensionless ratios $\sigma = 1$, $\delta = 1$ and $\eta = 0.15$, predicted by the linear and nonlinear in-plane vibration analysis. In this figure, the hypothesis of small static displacements is used for the nonlinear case. It is clearly observed from the figure that for the case of nonlinear analysis of the in-plane vibrations, the buckling phenomenon is removed from the results in the studied range of rotation speed as well as tune speeds. In Fig. 7 a comparison between in-plane and out-of-plane vibration frequencies of the rotating plate predicted by different static displacement assumptions is presented. This figure demonstrates a significant difference between predicted results for high values of rotation speeds, whereas for the case of small rotation velocities, the predicted results are in a good agreement. In addition, Fig. 7 suggests that nonlinear analysis of in-plane vibrations of the rotating plate results in a frequency modification for the out-of-plane vibration frequencies, since the static displacement predicted in this method is different from the one reported by the linear in-plane vibrations analysis.

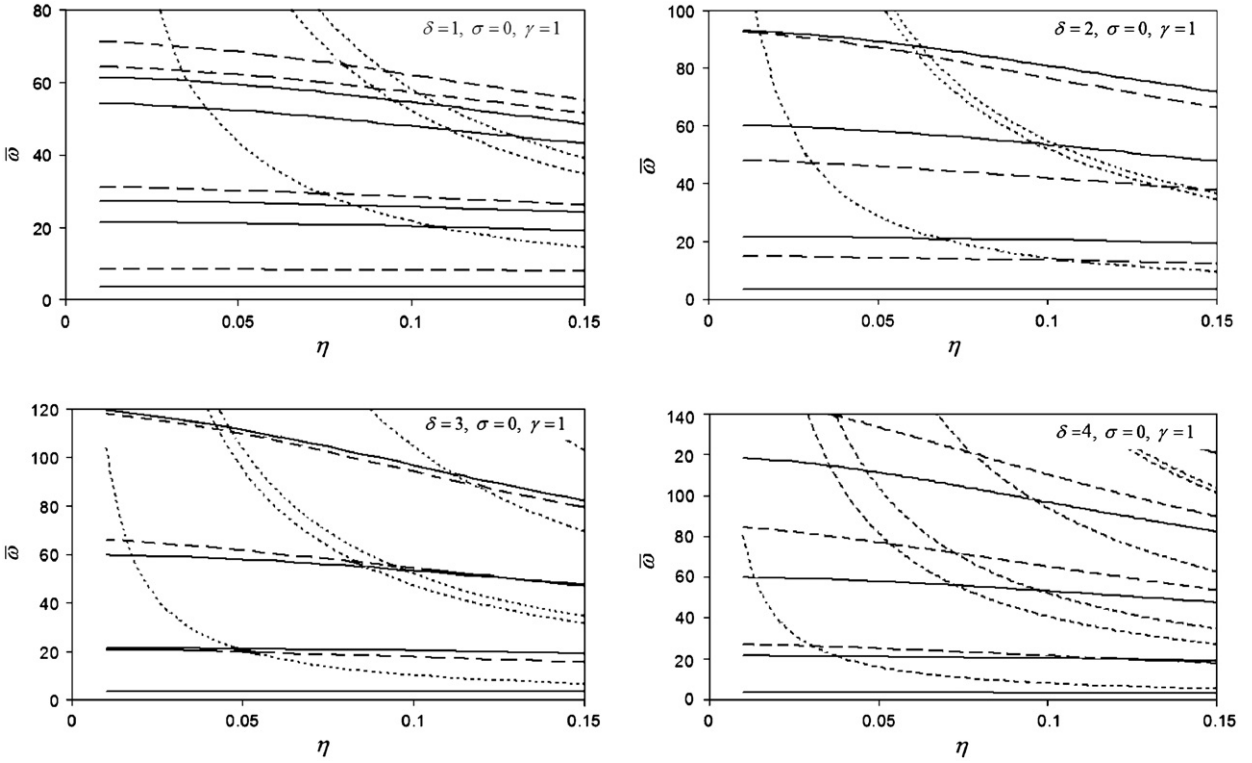

Fig. 4. Variations of the dimensionless natural frequencies of a rotating plate ($\gamma = 1$) versus thickness ratio (η) for different values of the aspect ratio (δ); — bending modes, -- torsional modes and ..... in-plane modes.

Fig. 8a shows the variations of the dimensionless natural frequencies versus hub radius ratio for a rotating plate with rotation speed $\gamma = 2$ and thickness ratio $\eta = 0.1$. The hypothesis of linear in-plane vibrations is used in this figure. It can be seen from the figure that, the out-of-plane frequencies (i.e. bending and torsional frequencies) increase as the hub radius increases, while the in-plane modes remain constant. The frequency result for the same plate and with the assumption of nonlinear in-plane vibrations with small moderate static displacements is presented in Fig. 8b. This figure shows the same results for the out-of-plane frequencies but a slot change in in-plane frequencies is observed in the figure. Since the rotation speed is small, the rate of changes in the in-plane frequencies is negligible. Fig. 8c presents the in-plane and out-of-plane frequencies of the plate for a higher value of rotation speed, still with the assumption of nonlinear in-plane vibrations with small moderate static displacements. For this case, one can see that the in-plane frequencies change more significantly.

Fig. 9 shows the in-plane vibration frequencies of a rotating plate with dimensionless ratios $\sigma = 0$, $\delta = 1$ and $\eta = 0.15$, predicted by nonlinear in-plane theory. The hypothesis of large static displacements is used in this figure. As it can be observed from the figure, the first in-plane vibration frequency of the plate reduces as the rotation speed increases. This frequency reduction ends to in-plane buckling phenomenon for fairly high rotation speeds. However, for such high rotation velocities, higher order nonlinear strain components must be used in Eq. (21b) since the static displacements would be considerably large. Practically, the rotating structure falls in static failure due to high in-plane stresses before attaining such high rotation speeds. Fig. 9 shows a tune speed for the rotating plate (point A) that must be avoided as described before.

5. Conclusions

A finite element method for vibration analysis of rotating thick plates is presented. Nonlinear equations of motion which contain Coriolis effects are obtained and then linearized using the conventional quasi-static

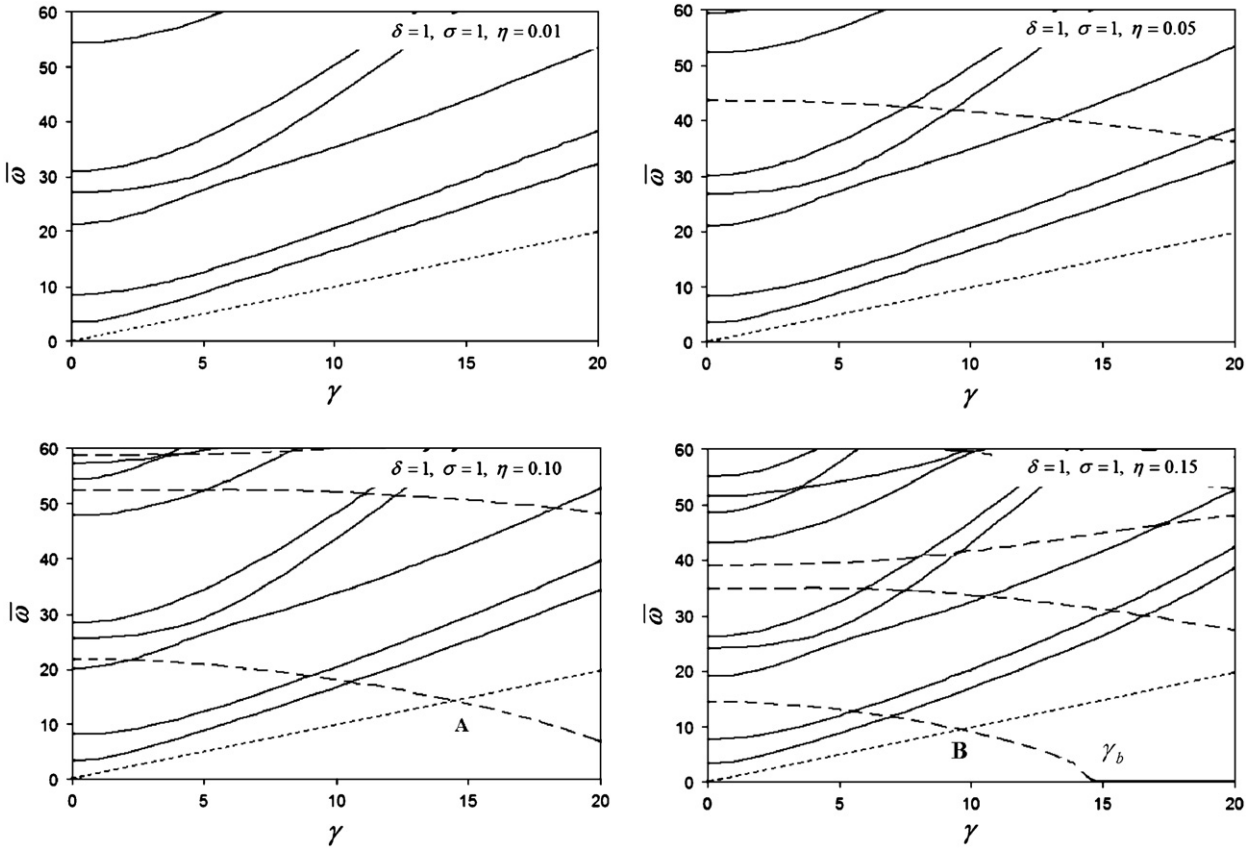

Fig. 5. Variations of the dimensionless natural frequencies versus dimensionless rotation speed γ; — out-plane modes, - - in-plane modes and ..... $\gamma = \overline{\omega}$.

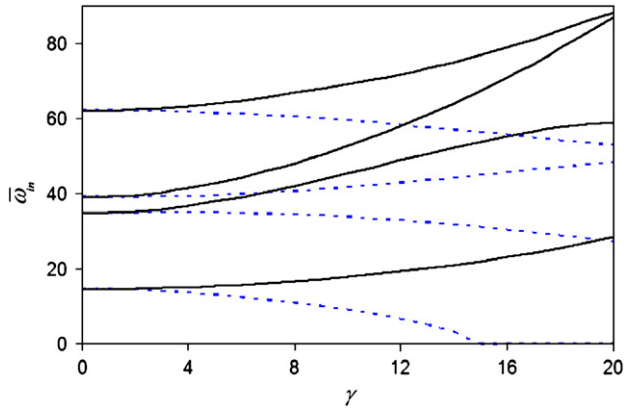

Fig. 6. In-plane vibration frequencies of a rotating plate with dimensionless ratios $\sigma = 0$, $\delta = 1$, $\eta = 0.15$; — nonlinear in-plane vibrations and ..... linear in-plane vibrations.

method. Out-of-plane and in-plane dimensionless natural frequencies of rotating plates are determined and discussed for different geometrical and dynamic parameters. The importance of nonlinear analysis of in-plane vibration behavior of rotating structures specially in high values of rotation speeds is demonstrated.

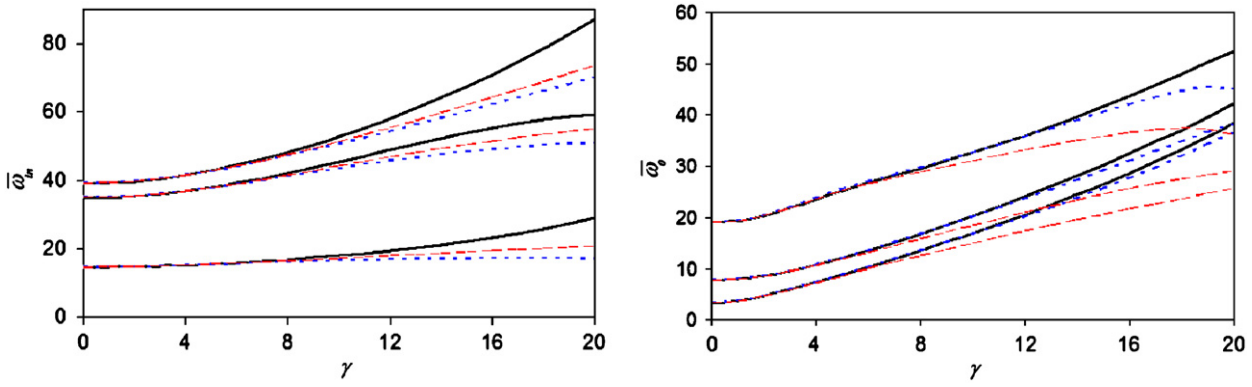

Fig. 7. In-plane ($\overline{\omega}_{\text{in}}$) and out-of-plane ($\overline{\omega}_o$) vibration frequencies of a rotating plate with dimensionless ratios $\sigma = 1$, $\delta = 1$ and $\eta = 0.15$; — small static displacements, ... moderate static displacements and -- large static displacements.

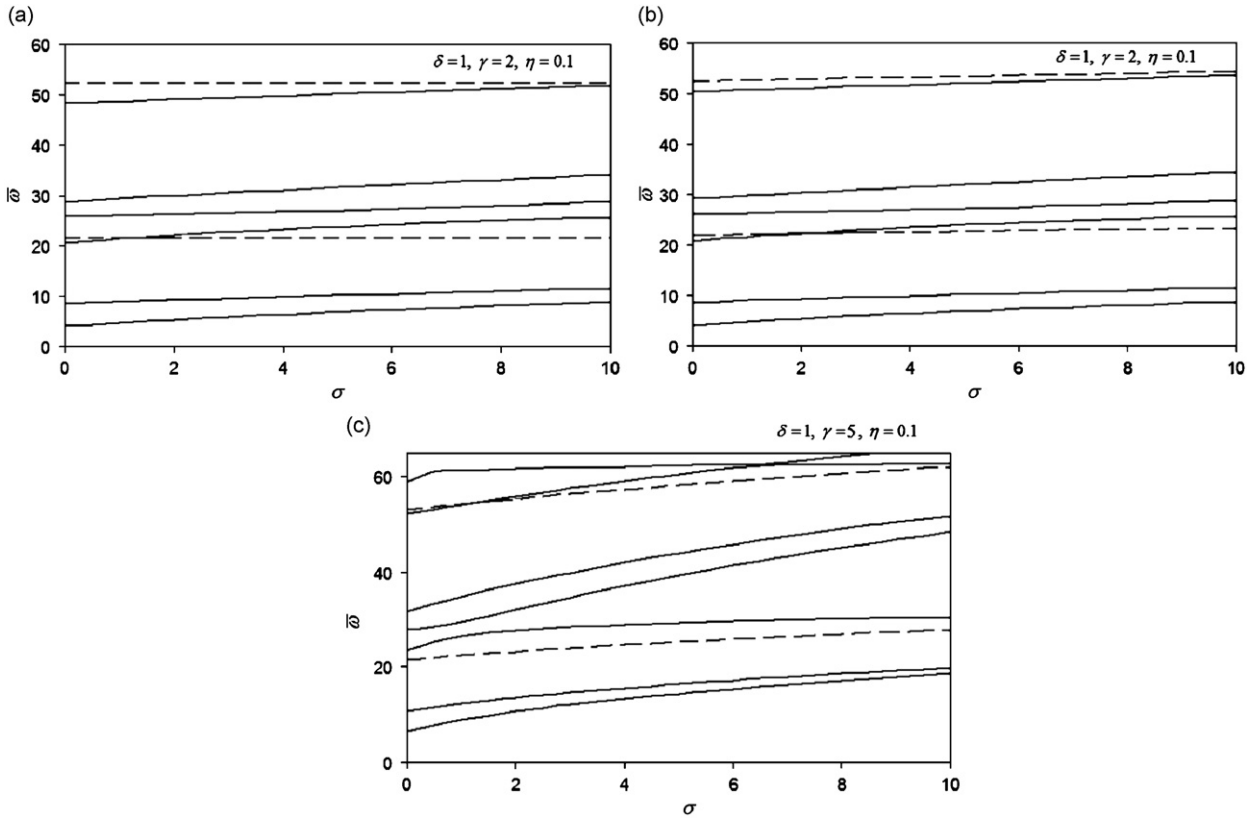

Fig. 8. Variations of the dimensionless natural frequencies versus hub radius ratioσpredicted by linear in-plane vibration analysis (a) and by nonlinear in-plane vibration analysis with small moderate static displacements (b, c); — out-plane modes and -- in-plane modes.

In addition, tune speeds are observed for in-plane frequencies where plate may fall in resonance in case of unbalanced rotor system. Furthermore loci crossing phenomenon is detected between in-plane and out-of-plane frequencies which are coupled through nonlinear terms in the governing equations.

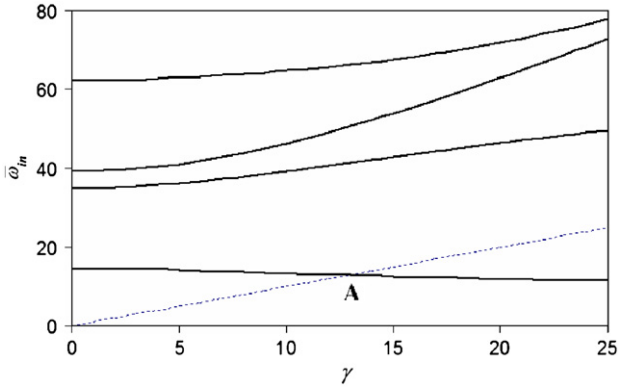

Fig. 9. In-plane vibration frequencies and tune speed of a rotating plate with dimensionless ratios $\sigma = 0$, $\delta = 1$ and $\eta = 0.15$.

Appendix A. Matrix of elastic coefficients

The matrix of elastic coefficients for isotropic Mindlin plates is defined as

$$\mathbf{C} = \begin{bmatrix} \frac{E}{1-v^2} & \frac{vE}{1-v^2} & 0 & 0 & 0 \\ \frac{vE}{1-v^2} & \frac{E}{1-v^2} & 0 & 0 & 0 \\ 0 & 0 & \frac{\kappa^2 E}{2(1+v)} & 0 & 0 \\ 0 & 0 & 0 & \frac{\kappa^2 E}{2(1+v)} & 0 \\ 0 & 0 & 0 & 0 & \frac{\kappa^2 E}{2(1+v)} \end{bmatrix}, \tag{A.1}$$

where κ is the Mindlin shear correction factor and it is equal to $(0.8667)^{0.5}$.

Appendix B. Operator matrices

The operator matrices introduced in Eq. (26) are defined as

$$\mathbf{B_1} = \begin{bmatrix} \frac{\partial}{\partial x} & 0 & 0 & z\frac{\partial}{\partial x} & 0 \\ 0 & \frac{\partial}{\partial y} & 0 & 0 & z\frac{\partial}{\partial y} \\ 0 & 0 & \frac{\partial}{\partial y} & 0 & 1 \\ 0 & 0 & \frac{\partial}{\partial x} & 1 & 0 \\ \frac{\partial}{\partial y} & \frac{\partial}{\partial x} & 0 & z\frac{\partial}{\partial y} & z\frac{\partial}{\partial x} \end{bmatrix}, \quad \mathbf{B_2} = \begin{bmatrix} \frac{\partial}{\partial x} & 0 & 0 & z\frac{\partial}{\partial x} & 0 \\ \frac{\partial}{\partial y} & 0 & 0 & z\frac{\partial}{\partial y} & 0 \\ 0 & \frac{\partial}{\partial x} & 0 & 0 & z\frac{\partial}{\partial x} \\ 0 & \frac{\partial}{\partial y} & 0 & 0 & z\frac{\partial}{\partial y} \\ 0 & 0 & \frac{\partial}{\partial x} & 0 & 0 \\ 0 & 0 & \frac{\partial}{\partial y} & 0 & 0 \end{bmatrix}, \tag{B.1}$$

$$\mathbf{A_1} = \begin{bmatrix} 0 & 0 & 0 & 0 & 0 \\ 0 & 0 & 0 & 0 & 0 \\ 0 & 0 & 0 & 0 & 0 \\ 0 & 0 & 0 & 0 & 0 \\ 0 & 0 & \frac{1}{2}\frac{\partial}{\partial x} & 0 & 0 \\ 0 & 0 & 0 & 0 & 0 \end{bmatrix}, \quad \mathbf{A_2} = \begin{bmatrix} 0 & 0 & 0 & 0 & 0 \\ 0 & 0 & 0 & 0 & 0 \\ 0 & 0 & 0 & 0 & 0 \\ 0 & 0 & 0 & 0 & 0 \\ 0 & 0 & 0 & 0 & 0 \\ 0 & 0 & \frac{1}{2}\frac{\partial}{\partial y} & 0 & 0 \end{bmatrix}, \tag{B.2a}$$

$$\mathbf{A_3} = \mathbf{A_4} = \begin{bmatrix} 0 & 0 & 0 & 0 & 0 \\ 0 & 0 & 0 & 0 & 0 \\ 0 & 0 & 0 & 0 & 0 \\ 0 & 0 & 0 & 0 & 0 \\ 0 & 0 & 0 & 0 & 0 \\ 0 & 0 & 0 & 0 & 0 \end{bmatrix}, \quad \mathbf{A_5} = \begin{bmatrix} 0 & 0 & 0 & 0 & 0 \\ 0 & 0 & 0 & 0 & 0 \\ 0 & 0 & 0 & 0 & 0 \\ 0 & 0 & 0 & 0 & 0 \\ 0 & 0 & \frac{\partial}{\partial y} & 0 & 0 \\ 0 & 0 & 0 & 0 & 0 \end{bmatrix}. \tag{B.2b}$$

In the case of full nonlinear strain components:

$$\mathbf{A_1} = \begin{bmatrix} \frac{1}{2}\frac{\partial}{\partial x} & 0 & 0 & \frac{z}{2}\frac{\partial}{\partial x} & 0 \\ 0 & 0 & 0 & 0 & 0 \\ 0 & \frac{1}{2}\frac{\partial}{\partial x} & 0 & 0 & \frac{z}{2}\frac{\partial}{\partial x} \\ 0 & 0 & 0 & 0 & 0 \\ 0 & 0 & \frac{1}{2}\frac{\partial}{\partial x} & 0 & 0 \\ 0 & 0 & 0 & 0 & 0 \end{bmatrix}, \quad \mathbf{A_2} = \begin{bmatrix} 0 & 0 & 0 & 0 & 0 \\ \frac{1}{2}\frac{\partial}{\partial y} & 0 & 0 & \frac{z}{2}\frac{\partial}{\partial y} & 0 \\ 0 & 0 & 0 & 0 & 0 \\ 0 & \frac{1}{2}\frac{\partial}{\partial y} & 0 & 0 & \frac{z}{2}\frac{\partial}{\partial y} \\ 0 & 0 & 0 & 0 & 0 \\ 0 & 0 & \frac{1}{2}\frac{\partial}{\partial y} & 0 & 0 \end{bmatrix}, \tag{B.3a}$$

$$\mathbf{A_3} = \begin{bmatrix} 0 & 0 & 0 & 0 & 0 \\ 0 & 0 & 0 & 1 & 0 \\ 0 & 0 & 0 & 0 & 0 \\ 0 & 0 & 0 & 0 & 1 \\ 0 & 0 & 0 & 0 & 0 \\ 0 & 0 & 0 & 0 & 0 \end{bmatrix}, \quad \mathbf{A_4} = \begin{bmatrix} 0 & 0 & 0 & 1 & 0 \\ 0 & 0 & 0 & 0 & 0 \\ 0 & 0 & 0 & 0 & 1 \\ 0 & 0 & 0 & 0 & 0 \\ 0 & 0 & 0 & 0 & 0 \\ 0 & 0 & 0 & 0 & 0 \end{bmatrix}, \tag{B.3b}$$

$$\mathbf{A_5} = \begin{bmatrix} \frac{\partial}{\partial y} & 0 & 0 & z\frac{\partial}{\partial y} & 0 \\ 0 & 0 & 0 & 0 & 0 \\ 0 & \frac{\partial}{\partial y} & 0 & 0 & z\frac{\partial}{\partial y} \\ 0 & 0 & 0 & 0 & 0 \\ 0 & 0 & \frac{\partial}{\partial y} & 0 & 0 \\ 0 & 0 & 0 & 0 & 0 \end{bmatrix}. \tag{B.3c}$$

References

[1] R. Southwell, F. Gough, The free transverse vibration of airscrew blades, British A.R.C. Reports and Memoranda 766, 1921.
[2] M. Schilhansl, Bending frequency of a rotating cantilever beam, *Journal of Applied Mechanics and Transactions of American Society of Mechanical Engineers* 25 (1958) 28–30.
[3] D.H. Hodges, M.J. Rutkowski, Free-vibration analysis of rotating beams by a variable-order finite-element method, *AIAA Journal* 19 (1981) 1459–1466.
[4] S.M. Lin, The instability and vibration of rotating beams with arbitrary pretwist and an elastically restrained root, *Journal of Applied Mechanics* 68 (2001) 844–853.
[5] E. Pesheck, C. Pierre, S.W. Shaw, Modal reduction of a nonlinear rotating beam through nonlinear normal modes, *Journal of Vibration and Acoustics* 124 (2002) 229–236.
[6] S.-Y. Oh, O. Song, L. Librescu, Effects of pretwist and presetting on coupled bending vibrations of rotating thin-walled composite beams, *International Journal of Solids and Structures* 40 (2003) 1203–1224.
[7] S.Y. Lee, S.M. Lin, C.T. Wu, Free vibration of a rotating non-uniform beam with arbitrary pretwist, an elastically restrained root and a tip mass, *Journal of Sound and Vibration* 273 (2004) 477–492.
[8] F.S.M. Jarrar, M.N. Hamdan, Nonlinear vibrations and buckling of a flexible rotating beam: a prescribed torque approach, *Mechanism and Machine Theory* 42 (2007) 919–939.
[9] H.H. Yoo, S.H. Shin, Vibration analysis of rotating cantilever beams, *Journal of Sound and Vibration* 212 (1998) 807–828.
[10] H.H. Yoo, J.H. Park, J. Park, Vibration analysis of rotating pre-twisted blades, *Computers and Structures* 79 (2001) 1811–1819.
[11] J. Chung, H.H. Yoo, Dynamic analysis of a rotating cantilever beam by using the finite element method, *Journal of Sound and Vibration* 249 (2002) 147–164.
[12] A.W. Leissa, Vibration of turbine engine blades by shell analysis, *The Shock and Vibration Digest* 12 (1980) 3–10.
[13] H.H. Yoo, S.K. Kim, Flapwise bending vibration of rotating plates, *International Journal for Numerical Methods in Engineering* 55 (2002) 785–802.
[14] M.A. Dokainish, S. Rawtani, Vibration analysis of rotating cantilever plates, *International Journal for Numerical Methods in Engineering* 3 (1971) 233–248.
[15] A. Karmakar, P.K. Sinha, Finite element free vibration analysis of rotating laminated composite pretwisted cantilever plates, *Journal of Reinforced Plastics and Composites* 16 (1997) 1461–1490.
[16] V. Ramamurti, R. Kielb, Natural frequencies of twisted rotating plates, *Journal of Sound and Vibration* 97 (1984) 429–449.
[17] H.H. Yoo, S.K. Kim, Free vibration analysis of rotating cantilever plates, *AIAA Journal* 40 (2002) 2188–2196.
[18] H.H. Yoo, C. Pierre, Modal characteristic of a rotating rectangular cantilever plate, *Journal of Sound and Vibration* 259 (2003) 81–96.
[19] R.D. Mindlin, Influence of rotary inertia and shear in flexural motion of isotropic elastic plates, *Journal of Applied Mechanics* 18 (1951) 31–38.
[20] T. Kane, D. Levinson, *Dynamics: Theory and Application*, McGraw-Hill, New York, 1985.
[21] M. Deshpande, C.D. Mote Jr., In-plane vibrations of a thin rotating disk, *Transactions of the ASME* 125 (2003) 68–72.
[22] J. Wauer, Discussion of in-plane vibrations of a thin rotating disk, *ASME Journal of Vibration and Acoustics* 126 (2004) 321.
[23] S.H. Hashemi, M. Arsanjani, Exact characteristic equations for some of classical boundary conditions of vibrating moderately thick rectangular plates, *International Journal of Solids and Structures* 42 (2005) 819–853.